Anisotropy in elastic properties of $TiSi_2$ (*C*49, *C*40 and *C*54), TiSi and Ti_5Si_3: an *ab-initio* density functional study

Materials Research Express

RECEIVED
22 May 2015

REVISED
28 July 2015

ACCEPTED FOR PUBLICATION
4 August 2015

PUBLISHED
1 September 2015

PAPER

Anisotropy in elastic properties of $TiSi_2$ (*C*49, *C*40 and *C*54), TiSi and Ti_5Si_3: an *ab-initio* density functional study

Manish K Niranjan

Department of Physics, Indian Institute of Technology, Hyderabad, India

E-mail: manish@iith.ac.in

Keywords: titanium silicides, elastic anisotropy, density functional theory

Abstract

We present a comparative study of the anisotropy in the elastic properties of the *C*49, *C*54 and *C*40 phases of $TiSi_2$, as well as orthorhombic TiSi and hexagonal Ti_5Si_3. The elastic constants, elastic moduli, Debye temperature and sound velocities are computed within the framework of density functional theory. The computed values of the elastic constants and moduli are found to be in excellent agreement with available experimental values. The average elastic moduli, such as Young's modulus, shear modulus, bulk modulus and Poisson's ratio, of polycrystalline aggregates are computed using the computed elastic constants of single crystals. The anisotropy in elastic properties is analyzed using estimates of shear anisotropic factors, bulk modulus anisotropic factors and variations in Young's and bulk moduli in different crystallographic directions. Among the Ti–Si phases, the computed directional Young's modulus profiles of *C*49 $TiSi_2$ and *C*40 $TiSi_2$ are found to be quite similar to those of bulk Si and Ti, respectively. In addition to the elastic properties, the electronic structure of five Ti–Si phases is studied. The density of states and planar charge density profiles reveal mixed covalent–metallic bonding in all Ti–Si phases.

1. Introduction

Transition metal silicides have played an important and crucial role in the development of microelectronics over the past three decades [1–7]. On the other hand, semiconducting silicides have been found to be promising for applications in photovoltaics [8], optoelectronics [9], and as thermoelectric materials [10]. Metal silicides are widely used as local interconnects and contacts to source, drain and gate regions in complementary metal–oxide–semiconductor (CMOS) devices because of their low resistivity, low contact resistance to silicon, high thermal stability, low electromigration and excellent process compatibility with standard silicon technology [1, 3, 6]. In CMOS devices, self-aligned silicide contacts (silicides) decrease the *RC* delay time of circuits due to the reduction in the parasitic, sheet, contact, and interconnect resistances within the source/drain regions and the polycrystalline silicon gate. This reduction in *RC* delay time, in turn, increases the speed performance of the device. Among all metal silicides, titanium disilicide ($TiSi_2$) has been one of the most widely used silicides for CMOS ultra-large-scale integration (ULSI) [1, 3]. In typical semiconductor device fabrication, $TiSi_2$ is formed by sputtering Ti film on a Si substrate followed by rapid thermal annealing of the film. At 550–700 °C, the high resistivity phase *C*49-$TiSi_2$ is formed first, followed by the desired low resistivity phase *C*54 $TiSi_2$ at a higher temperature of 750–850 °C [11–14]. However, in submicron Si lines, the transformation from *C*49 to *C*54 phase becomes difficult because of the low density of nucleation sites, rendering $TiSi_2$ unusable in submicron devices [15, 16]. Chen *et al* [17] have shown that a new metastable hexagonal *C*40 $TiSi_2$ phase is formed when Ti thin film deposited on Si substrate is annealed by pulsed laser annealing at a very high ramp rate and with very short duration. The *C*40 phase of $TiSi_2$ is formed primarily due to kinetic factors which result from the extreme thermal nonequilibrium induced by the pulsed laser annealing [12]. In addition to applications in microelectronics, $TiSi_2$ is also promising as an aero-space engineering material due to its low density, high hardness, high melting point, high creep strength and high oxidation resistance.

Over the years, the phases of $TiSi_2$, viz. *C*54, *C*49 and *C*40 grown on Si substrates have been studied experimentally in detail due to their practical importance. The electronic structures of these phases have also been studied theoretically by several groups [18–22]. However, theoretical and experimental studies of the elastic properties of different phases of $TiSi_2$ are scarce. Elastic properties of a material are important as they critically influence thin film growth on suitable substrates. Electronic and magnetic properties of thin films are also influenced by their elastic properties. Furthermore, elastic properties are related to various fundamental properties such as phonon spectra, equations of state, interatomic potentials, thermal expansion, specific heat, Gruneisen parameters, Debye temperature, etc. The strength of a material can be inferred from its elastic moduli, such as its Young's modulus, bulk modulus, shear modulus and Poisson ratio. Bonding features between various atoms and the stability of the system can be deduced from knowledge of the elastic constants. Furthermore, plastic properties of materials are associated with elastic properties. For instance, shear moduli along the slip planes of mobile dislocations influence plastic properties [19, 23]. Recently, the elastic properties of the *C*54 and *C*49 phases of orthorhombic $TiSi_2$ have been reported [19, 24]. However, no other work on the elastic properties of metastable phase *C*40 $TiSi_2$ has been reported to the best of our knowledge. The elastic properties of these phases of Ti–Si system are important, as they are expected to influence the microstructure and growth of Ti–Si thin films on Si substrates. In this article, we present a detailed *ab-initio* density-functional study of the elastic properties of five phases of titanium silicides: 1) orthorhombic *C*49 $TiSi_2$; 2) orthorhombic *C*54 $TiSi_2$; 3) hexagonal *C*40 $TiSi_2$; 4) orthorhombic *Pnma* TiSi and 5) hexagonal Ti_5Si_3. In particular, we calculate elastic constants, Debye temperatures, sound velocities, Poisson ratios and various moduli, such as Young's modulus, the bulk modulus, and the shear modulus. We also study the anisotropy in the elastic properties of different phases of $TiSi_2$, TiSi and Ti_5Si_3.

The rest of the paper is organized as follows. In section 2, we present the calculation methodology. Crystal and electronic structures are discussed in section 3. The elastic properties of single crystal and polycrystalline Ti–Si phases are discussed in sections 4 and 5, respectively. The anisotropy in elastic properties is computed in section 6. The sound velocities, Debye temperature and their relationship with elastic moduli are discussed in section 7. Concluding remarks are given in section 8.

2. Calculation methodology

We use density functional theory (DFT) [25] with the projected augmented wave (PAW) potentials [26], as implemented in the VASP package [27]. The Perdew–Burke–Ernzerhof (PBE) [28] form of generalized gradient approximation (GGA) is employed for the exchange and correlation potential. The Kohn–Sham wavefunctions are expanded in a plane wave basis set with a kinetic energy cutoff of 320 eV and higher. The Brillouin zones of *C*49 $TiSi_2$, *C*54 $TiSi_2$, *C*40 $TiSi_2$, *Pnma* TiSi and Ti_5Si_3 are sampled using $19 \times 5 \times 19$, $8 \times 14 \times 8$, $16 \times 16 \times 12$, $10 \times 18 \times 14$ and $10 \times 10 \times 14$ Monkhorst–Pack *k*-point meshes, respectively. The calculations are converged to 10^{-6} eV/cell and the structures are relaxed until the largest force becomes less than 10^{-2} eV $Å^{-1}$.

3. Crystal and electronic strcuture

*C*49 and *C*54 phases of $TiSi_2$ and TiSi crystallize in the orthorhombic structure with *Cmcm*, *Fddd* and *Pnma* space group symmetries, respectively. The crystal structures of *C*40 $TiSi_2$ and Ti_5Si_3 are hexagonal with $P6_222$ and $P6_3/mcm$ space group symmetries. The unit cells of these five Ti–Si systems are shown in figure 1. Tables 1 and 2 show the computed and experimental lattice constants, volume, fractional atomic coordinates, cohesive energies and heats of formation of the aforementioned Ti–Si phases. The calculated lattice constants and atomic coordinates are in good agreement and are within 1–2% of the available experimental values. The computed cohesive and formation energies of all five Ti–Si phases are ~6.4 eV/atom. Table 1 also lists the computed cohesive energies for bulk Si and Ti. As expected, the computed cohesive energies are overestimated as compared to experimental values. It can be seen that the computed values of cohesive energies of the Ti–Si phases are closer to those obtained for transition metals [29]. The magnitude and variation of the Ti–Si cohesive energies may be understood using a simple rectangular *d*-band model, where the shape of the *d*-band is assumed to be rectangular. In this model, cohesive energy depends on the width of the *d*-band and the number of electrons in it [30]. The formation energies of Ti–Si phases are computed to be ~0.6 eV/atom. Figure 2 shows the total density of states (DOS) of the Ti–Si phases. As evident, the DOS around the Fermi energy in $TiSi_2$ (*C*49, *C*54, *C*40), TiSi and Ti_5Si_3 are qualitatively similar. A dip in the DOS or deep valley (pseudogap) in the vicinity of the Fermi energy can also be seen in figure 2, indicating the presence of covalent bonding. It has been suggested that the Fermi energy position with respect to a valley or pseudogap and structural stability may be correlated [31]. The Fermi energy lies below the pseudogap in *C*54 and *C*40 $TiSi_2$, whereas it lies above the pseudogap in *C*49 $TiSi_2$. It is interesting to note that the position of the

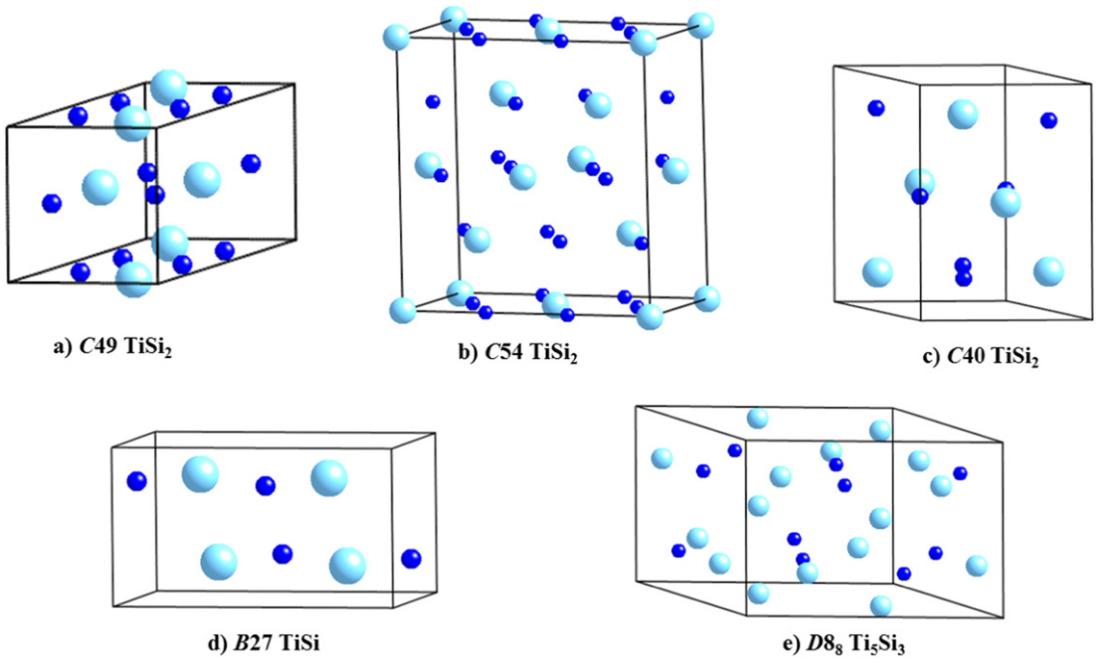

Figure 1. The unit cells of (**a**) *C*49 $TiSi_2$ (**b**) *C*54 $TiSi_2$ (**c**) *C*40 $TiSi_2$ (**d**) B27 (*Pnma*) TiSi (**e**) Ti_5Si_3. Ti and Si atoms are indicated by larger red and smaller blue balls, respectively.

Table 1. Calculated and experimental lattice constants, volume, cohesive energy (eV/atom) and heat of formation (eV/atom), of *C*49, *C*54, *C*40 $TiSi_2$, *Pnma* TiSi and Ti_5Si_3.

Composition	Structure		*a* (Å)	*b* (Å)	*c* (Å)	V_0(Å^3)	E_{coh}	ΔH
$TiSi_2$	*C*49	Cal.	3.543	13.544	3.578	171.7	6.45	0.56
		Exp.[44]	3.55	13.49	3.55	170.0	—	—
$TiSi_2$	*C*54	Cal.	8.257	4.801	8.559	339.3	6.34	0.55
		Exp.[49]	8.27	4.80	8.55	339.4	—	—
$TiSi_2$	*C*40	Cal.	4.727	4.727	6.587	127.5	6.33	0.54
		Exp.[45]	4.71	4.71	6.53	125.5	—	—
TiSi	*B*27	Cal.	6.528	3.643	5.005	119.0	6.76	0.77
		Exp.[46]	6.54	3.63	4.99	118.5	—	—
Ti_5Si_3	$D8_8$	Cal.	7.463	7.463	5.123	247.1	6.34	0.55
		Exp.	—	—	—	—	—	—
Si		Cal.	5.466			40.84	5.36	
		Exp.[32,47]	5.431			40.05	4.63	
Ti		Cal.	2.930		4.646	34.54	6.62	
		Exp.[32,48]	2.951		4.684	35.32	4.85	

Fermi energy and pseudogap coincides in *Pnma* TiSi. The DOS at the Fermi energy is the highest for Ti_5Si_3 which is expected due to more Ti 3*d* states hybridizing with Si 2*p* states. It can also be seen in figure 2 that a gap opens up in the valence band of TiSi and Ti_5Si_3, around ~5 eV below the Fermi energy. In figure 3, the charge difference density contours are shown for *C*49 $TiSi_2$ (100) and *C*54 $TiSi_2$ (001) planes. For comparison with pure covalent and metallic bonding, charge contours are also shown for Si(1-10) and Ti(1-10) planes. Figure 3 shows that weak directional bonds are formed between Ti and Si atoms whereas Si–Si atoms exhibit strong directional bonds. The bonding between atoms in other Ti–Si phases are found to be similar qualitatively.

4. Single crystal elastic constants

The relationship between elastic constants C_{ijkl}, stress σ_{ij} and strain ε_{kl} is given as follows [32]:

$$\sigma_{ij} = \sum_{k=1}^{3}\sum_{l=1}^{3} C_{ijkl}\varepsilon_{kl} \qquad (i, j = 1,2,3). \tag{1}$$

Table 2. Calculated and experimental atomic fractional coordinates of *C*49, *C*54, *C*40 $TiSi_2$, *Pnma* TiSi and Ti_5Si_3.

Composition	Structure	Sp. gr.	site		*u*	*v*	*w*
$TiSi_2$	*C*49	*Cmcm*	Ti	Cal.	0.0000	0.1031	0.2500
				Exp.	0.0000	0.1022	0.2500
			Si_1	Cal.	0.0000	0.4408	0.2500
				Exp.	0.0000	0.4461	0.2500
			Si_2	Cal.	0.0000	0.7503	0.2500
				Exp.	0.0000	0.7523	0.2500
$TiSi_2$	*C*54	*Fddd*	Ti	Cal.	0.0000	0.0000	0.0000
				Exp.	0.0000	0.0000	0.0000
			Si	Cal.	0.3369	0.0000	0.0000
				Exp.	0.3365	0.0000	0.0000
$TiSi_2$	*C*40	$P6_222$	Ti	Cal.	0.5000	0.5000	0.5000
				Exp.	—	—	—
			Si	Cal.	0.1623	0.3245	0.5000
				Exp.	—	—	—
TiSi	*B*27	*Pnma*	Ti	Cal.	0.1759	0.2500	0.1286
				Exp.	0.1790	0.2500	0.1270
			Si	Cal.	0.0442	0.2500	0.6458
				Exp.	0.0300	0.2500	0.6200
Ti_5Si_3	$D8_8$	$P6_3/mcm$	Ti1	Cal.	0.3333	0.6667	0.0000
				Exp.	0.3333	0.6667	0.0000
			Ti2	Cal.	0.2501	0.0000	0.2500
				Exp.	0.2400	0.0000	0.2500
			Si	Cal.	0.6080	0.0000	0.2500
				Exp.	0.6150	0.0000	0.2500

Equation (1) in Voigt notation ($11 \rightarrow 1, 22 \rightarrow 2, 33 \rightarrow 3, 12 \rightarrow 6, 13 \rightarrow 5, 23 \rightarrow 4$) can be written as:

$$\sigma_\alpha = \sum_{\beta=1}^{6} C_{\alpha\beta}\varepsilon_\beta \qquad (\beta = 1{-}6). \tag{2}$$

The strain tensor in matrix form is given as:

$$\varepsilon = \begin{bmatrix} e_1 & e_6/2 & e_5/2 \\ e_6/2 & e_2 & e_4/2 \\ e_5/2 & e_4/2 & e_3 \end{bmatrix}. \tag{3}$$

The energy of the crystal under small deformation can be written in terms of strain and external stress as [32]:

$$E = E_0 + V\sum_{\alpha=1}^{6}\sigma_\alpha e_\alpha + \frac{V}{2}\sum_{\alpha,\beta=1}^{6} C_{\alpha\beta}e_\alpha e_\beta. \tag{4}$$

The second term in equation (4) is zero in our calculations since an undistorted crystal is taken as the equilibrium structure at zero pressure. The numbers of independent elastic constants in the case of orthorhombic (*C*49, *C*54 $TiSi_2$ and *Pnma* TiSi), and hexagonal (*C*40 $TiSi_2$ and Ti_5Si_3) structures are nine and six, respectively. Table 3 shows the computed elastic constants of $TiSi_2$ (*C*49, *C*54 and *C*40), *Pnma* TiSi, and Ti_5Si_3. Table 3 also lists the reported experimental values for *C*54 $TiSi_2$. As evident, the computed values are in excellent agreement with the experimental values. The computed elastic constants and bulk moduli of bulk Ti and Si are within ~10% and ~7% of the experimental values. The single crystal bulk modulus of orthorhombic and hexagonal systems can be expressed in terms of elastic constants as:

$$B_0^{\text{orthogonal}} = \left(C_{11} + C_{22} + C_{33} + 2C_{12} + 2C_{13} + 2C_{23}\right)/9 \tag{5}$$

$$B_0^{\text{hexagonal}} = \left(2C_{11} + C_{33} + 2C_{12} + 4C_{13}\right)/9 \tag{6}$$

The bulk modulus can also be computed by fitting the total energy as a function of volume to a four-term Birch–Murnaghan equation of state [33].

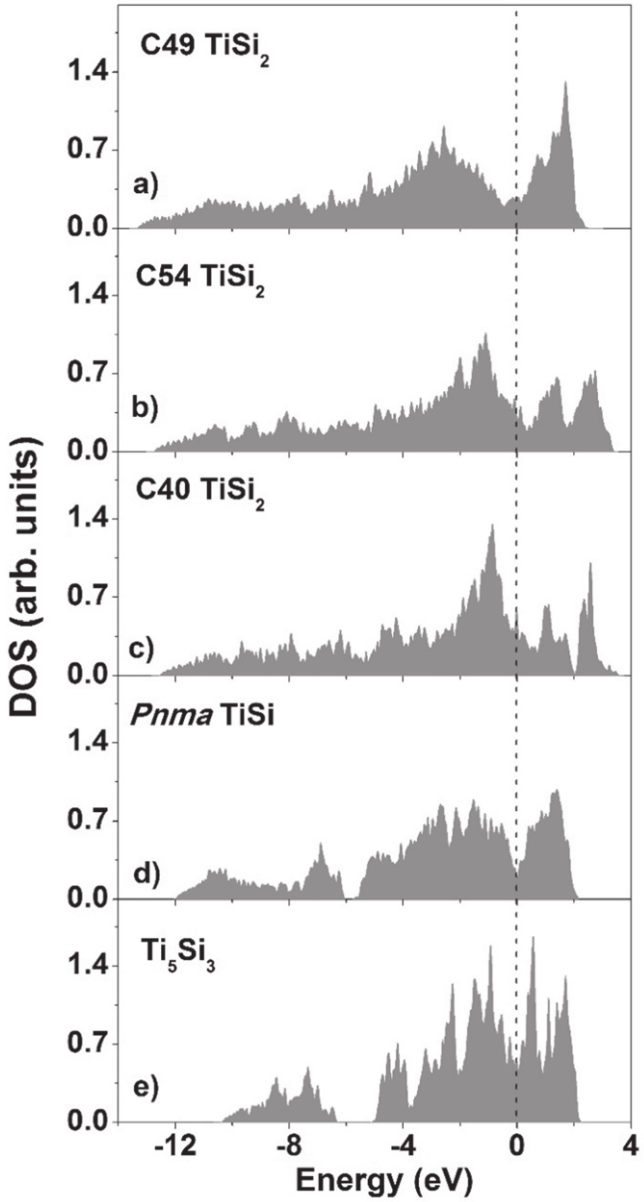

Figure 2. The total density of states in (**a**) *C*49 $TiSi_2$ (**b**) *C*54 $TiSi_2$ (**c**) *C*40 $TiSi_2$ (**d**) *Pnma* TiSi (**e**) Ti_5Si_3. The Fermi energy is indicated by the vertical line.

$$E(V) = \sum_{n=1}^{4} c_n V^{-2n/3}; \qquad B_0^{B-M} = V_0 \frac{\partial^2 E(V)}{\partial V^2}\bigg|_{V=V_0} \tag{7}$$

As is clear from table 3, the bulk moduli calculated from the Birch–Murnaghan fit and from equations (5) and (6) are in excellent agreement within ~1%, indicating internal consistency in the calculations.

5. Elastic properties of polycrystalline system

Though it is not possible to measure the individual elastic constants (C_{ij}) of polycrystalline systems, average elastic properties, such as the polycrystalline Young's modulus (E), Poisson's ratio (ν), the bulk modulus (B), the shear modulus (G), etc, can be computed using single crystal elastic constants [19, 34].

The polycrystalline Young's modulus E and Poisson's ratio ν are given by:

$$E = \frac{9B_H G_H}{3B_H + G_H} \qquad \nu = \frac{3B_H - 2G_H}{2\left(3B_H + G_H\right)}. \tag{8}$$

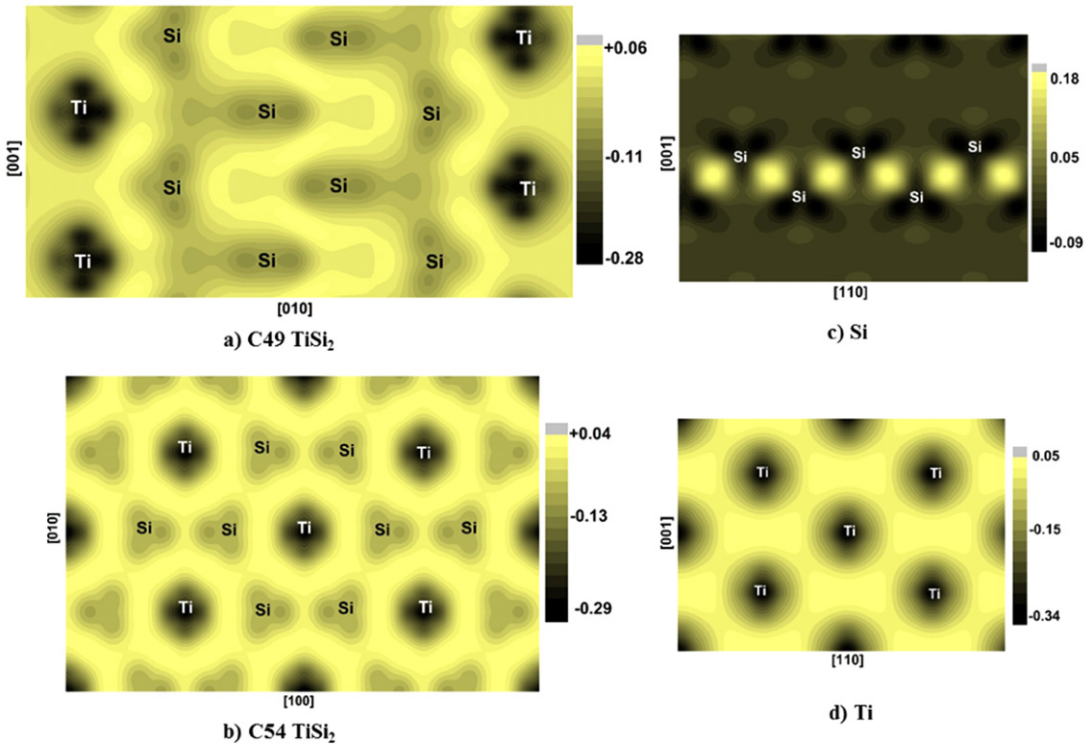

Figure 3. Valence electron charge density contours (**a**) in (100) plane of *C*49 $TiSi_2$ unit cell (**b**) in (001) plane of *C*54 $TiSi_2$ unit cell (**c**) in (1-10) plane of bulk Si unit cell (**d**) in (1-10) plane of Ti unit cell.

Table 3. Calculated and experimental elastic constants and bulk moduli (in GPa) of *C*49, *C*54, *C*40 $TiSi_2$, *Pnma* TiSi and Ti_5Si_3, Ti and Si. $B_0^{B\text{-}M}$ and $B_0^{elastic}$ indicate bulk modulus calculated using a Birch–Murnaghan fit and single crystal elastic constants, respectively. Experimental elastic constants for *C*49 $TiSi_2$ are taken from [49].

		*C*49 $TiSi_2$	*C*54 $TiSi_2$	*C*40 $TiSi_2$	*Pnma* TiSi	$D8_8$ Ti_5Si_3	Ti	Si
C_{11}	Cal.	270.0	321.5	314.8	227.8	286.9	180.7	153.8
	Exp.	—	317.5	—	—	—	162.4	165
C_{22}	Cal.	188.5	317.3		279.2			
	Exp.	—	320.4	—	—	—		
C_{33}	Cal.	307.8	408.7	395.6	315.4	270.5	188.8	
	Exp.	—	413.2	—	—	—	180.7	
C_{44}	Cal.	121.1	112.4	89.5	95.9	94.04	45.2	75.8
	Exp.	—	112.5	—	—	—	46.7	79.1
C_{55}	Cal.	138.5	75.5	—	97.3	—		
	Exp.	—	75.8	—	—	—		
C_{66}	Cal.	112.6	123.7	128.7	150.4	88.5	49.0	
	Exp.	—	117.5	—	—	—		
C_{12}	Cal.	60.2	28.1	57.4	109.6	109.9	82.8	57.3
	Exp.	—	29.3	—	—	—	92.0	63
C_{13}	Cal.	102.8	22.9	43.7	79.5	56.4	79.8	
	Exp.	—	38.4	—	—	—	69.0	
C_{23}	Cal.	65.5	82.5	—	71.7	—		
	Exp.	—	86.0	—	—	—		
$B_0^{B\text{-}M}$	Cal.	134.3	145.2	145.3	148.5	142.1	114.4	88.9
$B_0^{elastic}$	Cal.	135.9	146.1	146.1	149.3	143.3	115.0	89.4
B_0	Exp.			146.8				97

Here, B_H and G_H are the bulk and shear moduli in Hill's approximation [35–37], which in turn are averages of Voigt and Reuss values of bulk (B_V and B_R) and shear (G_V and G_R) moduli.

$$B_H = \frac{1}{2}\left(B_R + B_V\right); \qquad G_H = \frac{1}{2}\left(G_R + G_V\right). \tag{9}$$

Table 4. Calculated shear (G) modulus and bulk moduli (B) (in GPa) in Hill's approximation, Young modulus (E) (in GPa), Poisson's ratio (ν), and bulk modulus (B) (in GPa) along [100], [010] and [001] of $C49$, $C54$, $C40$ $TiSi_2$, *Pnma* TiSi and Ti_5Si_3, Ti and Si.

		G_H	B_H	E	ν	$B_{[100]}$	$B_{[010]}$	$B_{[001]}$
$C49$ $TiSi_2$	Cal.	107.7	127.1	253.9	0.18	460.7	247.9	600.4
$C54$ $TiSi_2$	Cal.	118.8	144.4	279.7	0.18	361.1	410.0	555.9
$C40$ $TiSi_2$	Cal.	116.9	145.6	276.7	0.18	407.6	407.6	503.7
Pnma TiSi	Cal.	102.8	148.8	250.7	0.22	367.2	502.5	492.1
$D8_8$ Ti_5Si_3	Cal.	96.5	142.5	236.2	0.22	471.5	471.5	355.5
Ti	Cal.	48.3	115.0	127.1	0.32	339.6	339.6	356.2
	Exp.			116	0.32			
Si	Cal.	63.2	89.5	153.5	0.22	268.4	268.4	268.4
	Exp.			150	0.22			

In the Reuss and Voigt schemes, uniform stress and strain in polycrystalline aggregates are taken to be equal to external strain and stress, respectively. The Reuss shear modulus (G_R) and the Voigt shear modulus (G_V) can be obtained from components of the compliance (S) and elastic matrices (C). In the case of orthorhombic crystals G_R and G_V are given as:

$$G_R = 15\Big[4\big(S_{11} + S_{22} + S_{33}\big) + 3\big(S_{44} + S_{55} + S_{66}\big) - 4\big(S_{12} + S_{13} + S_{23}\big)\Big]^{-1} \tag{10}$$

$$G_V = \frac{1}{15}\Big[C_{11} + C_{22} + C_{33} - C_{12} - C_{13} - C_{23}\Big] + \frac{3}{15}\Big[C_{44} + C_{55} + C_{66}\Big] \tag{11}$$

Similarly, the bulk modulus in the Reuss (B_R) and Voigt (B_V) approximations is given by:

$$B_R = \Big[S_{11} + S_{22} + S_{33} + 2S_{12} + 2S_{13} + 2S_{23}\Big]^{-1} \tag{12}$$

$$B_V = \big(C_{11} + C_{22} + C_{33} + 2C_{12} + 2C_{13} + 2C_{23}\big)/9 \tag{13}$$

It has been suggested that the bulk and shear moduli in the Reuss and Voigt approximations are close to the lower and upper bounds of true polycrystalline bulk and shear moduli. Thus, the computed values in Hill's approximation are expected to provide more practical estimates for the moduli of polycrystalline materials. The computed bulk and shear moduli in Hill's approximation, Young's moduli and Poisson's ratios of five Ti–Si systems are listed in table 4. The relatively large values of shear moduli of listed Ti–Si phases are indicative of pronounced directional bonding which can also be seen in figure 3. As can be seen in table 4, the computed values of Young's modulus for Si and Ti are in good agreement with the experimental values. Poisson's ratio (ν) is indicative of stability against shear. The small value of Poisson's ratio of the Ti–Si phases shows that these phases are relatively stable against shear. It can be seen in table 4 that the computed values of Poisson's ratio for Ti and Si are in excellent agreement with experimental values. The ratio of the bulk modulus to the shear modulus (B/G) can be used to infer ductile or brittle characteristics of polycrystalline phases [38]. On the other hand, resistance to fracture and plastic deformation can be assessed from the magnitude of the bulk and shear modulus, respectively. High and low values of B/G are indicative of ductility and brittleness, respectively, with a critical value of $\sim$1.75. For all listed Ti–Si phases in table 4, B/G is computed to be less than 1.75, suggesting the brittle nature of them. The Young's modulus of the listed Ti–Si phases in table 4 is higher than that of pure Ti and Si. The Poisson's ratio of the $TiSi_2$ phases ($C49$, $C54$ and $C40$) is smaller than that of Ti and Si. In the case of *Pnma* TiSi and Ti_5Si_3, the Poisson's ratio is smaller than that of Ti, but almost equal to that of Si. The Poisson's ratio may also provide information on the nature of bonding forces, since it is related to volume change during uniaxial deformation [39]. For central force solids, the magnitude of Poisson's ratio lies between 0.25 and 0.5. The computed Poisson's ratio of 0.18 for $TiSi_2$ phases and 0.22 for TiSi and Ti_5Si_3 phases suggests that interatomic forces in Ti–Si phases are non-central in nature. It is apparent from tables 3 and 4 that all five phases of Ti–Si exhibit qualitatively similar trends in average elastic properties.

6. Elastic anisotropy

The understanding of anisotropy in elastic properties is important in that it influences various physical properties, microstructure and growth of thin films [19, 40]. Shear anisotropic factors can be used to estimate the degree of anisotropy in atomic bonding in different planes. The shear anisotropic factor A_1 for the $\{100\}$ shear planes between $\langle 011\rangle$ and $\langle 010\rangle$ is given by:

Table 5. Calculated shear elastic anisotropic factors (A_1, A_2, and A_3), directional bulk modulus anisotropy factors (A_{Ba}, and A_{Bc}), and percent compressibility and shear moduli factors (A_B and A_G) of *C*49, *C*54, *C*40 $TiSi_2$, *Pnma* TiSi and Ti_5Si_3, Ti and Si.

	A_1	A_2	A_3	A_{Ba}	A_{Bc}	A_B	A_G
*C*49 $TiSi_2$	1.30	1.52	1.33	1.86	2.42	3.4	2.4
*C*54 $TiSi_2$	0.66	0.54	0.85	0.88	1.36	1.2	3.7
*C*40 $TiSi_2$	0.57	0.57	1.00	1.00	1.23	1.2	3.7
Pnma TiSi	1.00	0.86	2.09	0.73	0.98	0.4	3.3
$D8_8$ Ti_5Si_3	0.85	0.85	1.00	1.00	0.75	0.5	0.7
Ti	0.86	0.86	1.0	1.0	1.1	0.1	1.7
Si	1.57	1.57	1.57	1.0	1.0	0.0	2.4

$$A_1 = 4C_{44}\left(C_{11} + C_{33} - 2C_{13}\right)^{-1} \tag{14}$$

Similarly, shear anisotropic factors A_2 and A_3 for the {010} shear plane (⟨001⟩ and ⟨101⟩) and {001} shear plane (⟨010⟩ and ⟨110⟩), respectively, are given by:

$$A_2 = 4C_{55}\left(C_{22} + C_{33} - 2C_{23}\right)^{-1} \qquad A_3 = 4C_{66}\left(C_{11} + C_{22} - 2C_{12}\right)^{-1} \tag{15}$$

Table 5 shows computed shear anisotropic factors for five Ti–Si phases. The magnitude of the shear anisotropic factors is one for isotropic crystals. The anisotropy can be estimated from the deviation of the shear anisotropic factors from a magnitude of one. The shear anisotropic factors (A_1, A_2 A_3) of the *C*49 phase are smaller and larger than those for the orthorhombic *C*49 and *C*54 phases of $TiSi_2$. The A_1 and A_2 factors are smaller than those for hexagonal *C*40 $TiSi_2$, whereas the A_3 component is of the magnitude one, as expected. In the case of orthorhombic *Pnma* TiSi, A_2 and A_3 are smaller and larger than one, whereas A_1 is almost one. The A_1 and A_2 factors are smaller than one for hexagonal Ti_5Si_3, whereas the A_3 component is one. The shear anisotropic factors of Ti and Si are also listed in table 5. As can be seen, the shear anisotropic factors are smaller and larger for Ti and Si, respectively. A_3 for hexagonal Ti is one, as expected. Additionally, elastic anisotropy can also result from anisotropy in the bulk modulus. The directional bulk modulus *B* is computed using the following relation [19, 34]:

$$B = \left[\left(S_{11} + S_{12} + S_{13}\right)l_1^2 + \left(S_{21} + S_{22} + S_{23}\right)l_2^2 + \left(S_{31} + S_{32} + S_{33}\right)l_3^2\right]^{-1} \tag{16}$$

where l_1, l_2 and l_3 are direction cosines and S_{ij} are components of the elastic compliance matrix. Figure 4 shows a three-dimensional representation of the computed bulk modulus of the Ti–Si systems along different directions. The anisotropy in bulk modulus is reflected in the nonspherical shape of the directional bulk modulus. As evident from figure 4, the anisotropy in bulk modulus is similar in all five Ti–Si phases. The computed bulk moduli along the [100], [010] and [001] directions are listed in table 4. The bulk modulus anisotropy factors along the *a* ([100]) and *c* ([001]) axes can be computed as [19, 34]

$$A_{B_a} = B_a/B_b; \qquad A_{B_c} = B_c/B_b \tag{17}$$

Table 5 shows the bulk anisotropy factors for five Ti–Si phases. For the elastically isotropic crystal, the magnitude of these factors is one. Among the listed Ti–Si phases, the computed magnitude of the bulk anisotropy factors is largest for the *C*49 $TiSi_2$ phase (see table 5 and figure 4). Also listed in table 5 are the percent shear and compressibility elastic anisotropies, which are defined as follows in terms of the Voigt and Reuss shear and bulk moduli [41]:

$$A_G = \frac{G_V - G_R}{G_V + G_R}, \qquad A_B = \frac{B_V - B_R}{B_V + B_R} \tag{18}$$

The values of A_G and A_B are bounded by 0% and 100% limits which indicate elastic isotropy and the highest possible anisotropy, respectively. The percent shear anisotropy (A_G) is ∼3.7% for *C*54 $TiSi_2$, *C*40 $TiSi_2$ and *Pnma* TiSi. For *C*49 $TiSi_2$, the computed value of A_G is ∼2.4%, whereas it is ∼0.7% for Ti_5Si_3. The computed percent compressibility anisotropy (A_B) is highest (∼3.4%) for *C*49 $TiSi_2$ and smallest (∼0.4%) for *Pnma* TiSi. The variation in Young's modulus along different directions can also be used to infer the degree of anisotropy in elastic properties. For an orthorhombic crystal, the Young's modulus *E* in an arbitrary direction with direction cosines l_1, l_2, and l_3 can be computed as [19, 23, 34]

$$E = \left(l_1^4 S_{11} + 2l_1^2 l_2^2 S_{12} + 2l_1^2 l_3^2 S_{13} + l_2^4 S_{22} + 2l_2^2 l_3^2 S_{23} + l_3^4 S_{33} + l_2^2 l_3^2 S_{44} + l_1^2 l_3^2 S_{55} + l_1^2 l_2^2 S_{66}\right)^{-1} \tag{19a}$$

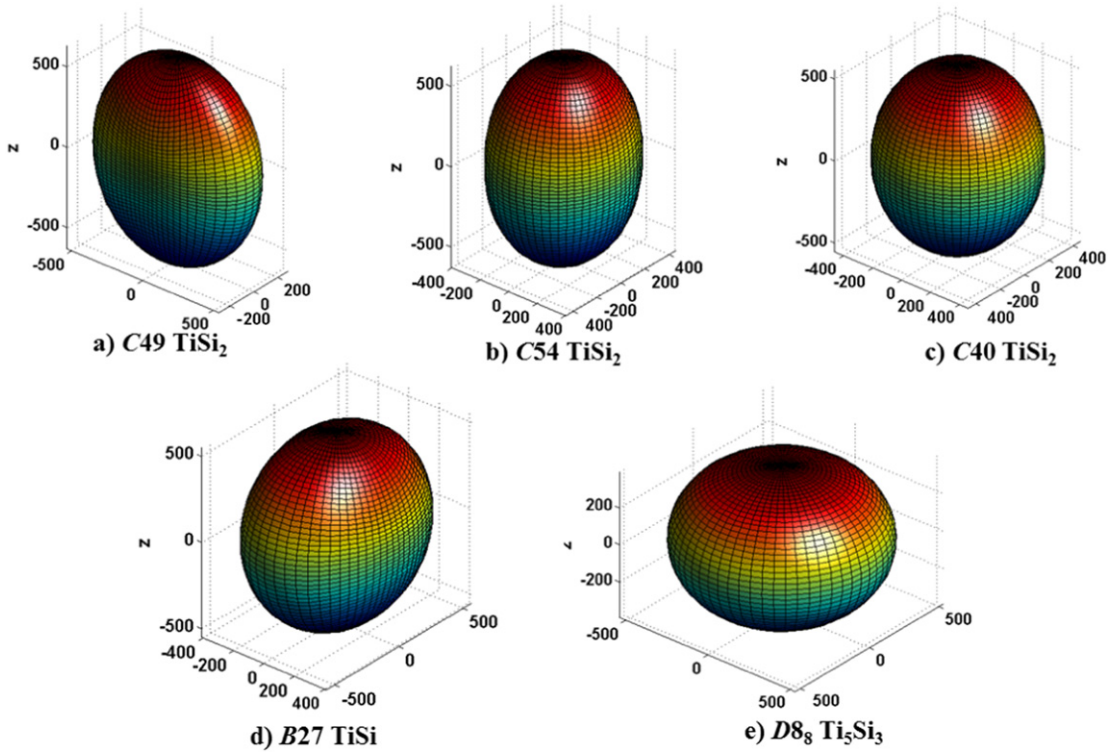

Figure 4. Direction dependent bulk modulus (B) of (**a**) $C49$ $TiSi_2$ (**b**) $C54$ $TiSi_2$ (**c**) $C40$ $TiSi_2$ (**d**) *Pnma* TiSi (**e**) Ti_5Si_3.

Table 6. Young's modulus (in GPa) along [100], [010], [001] and [111] directions of $C49$, $C54$, $C40$ $TiSi_2$, *Pnma* TiSi and Ti_5Si_3, Ti and Si.

	E_{100}	E_{010}	E_{001}	E_{111}
$C49$ $TiSi_2$	227.2	168.3	258.3	279.3
$C54$ $TiSi_2$	318.4	298.9	386.5	241.7
$C40$ $TiSi_2$	301.0	301.0	385.3	243.1
Pnma TiSi	175.9	222.6	282.8	263.9
$D8_8$ Ti_5Si_3	240.1	240.1	254.5	228.4
Ti	130.6	130.6	140.5	122.7
Si	122.7	122.7	122.7	177.3

where S_{ij} are components of the elastic compliance matrix. Table 6 shows the computed Young's moduli of Ti–Si phases along the [100], [010], [001] and [111] directions. Figure 5 shows a plot of the directional Young's modulus along different directions. The directional bulk and Young's modulus for bulk Si and Ti are shown in figure 6. As can be seen in figures 5 and 6, the shape of the directional Young's modulus profile for $C49$ $TiSi_2$ and $C40$ $TiSi_2$ is similar to that for bulk Si and Ti. The computed ratio between Young's modulus along [111] and [100] is 1.23 for $C49$ $TiSi_2$, 0.76 for $C54$ $TiSi_2$, 0.81 for $C40$ $TiSi_2$, 1.50 for *Pnma* TiSi, 0.95 for Ti_5Si_3, 0.94 for Ti and 1.44 for Si. The ratio between Young's modulus along [001] and [100] is 1.14, 1.21, 1.28, 1.61, 1.06, 1.08 and 1.0 in respective order. It is evident from tables 5 and 6 and figures 4 and 5, that the five Ti–Si phases exhibit moderate anisotropy in elastic properties.

7. Debye temperature

The Debye temperature is related to the average sound velocity as follows [42]:

$$\theta_D = \frac{h}{k_B}\left(\frac{3}{4\pi V_a}\right)^{1/3} v_m \qquad (19b)$$

where V_a, v_m h, and k_B, are atomic volume, sound velocity Planck's constant and Boltzmann's constant, respectively. The average sound velocity in polycrystalline materials is given as [42]

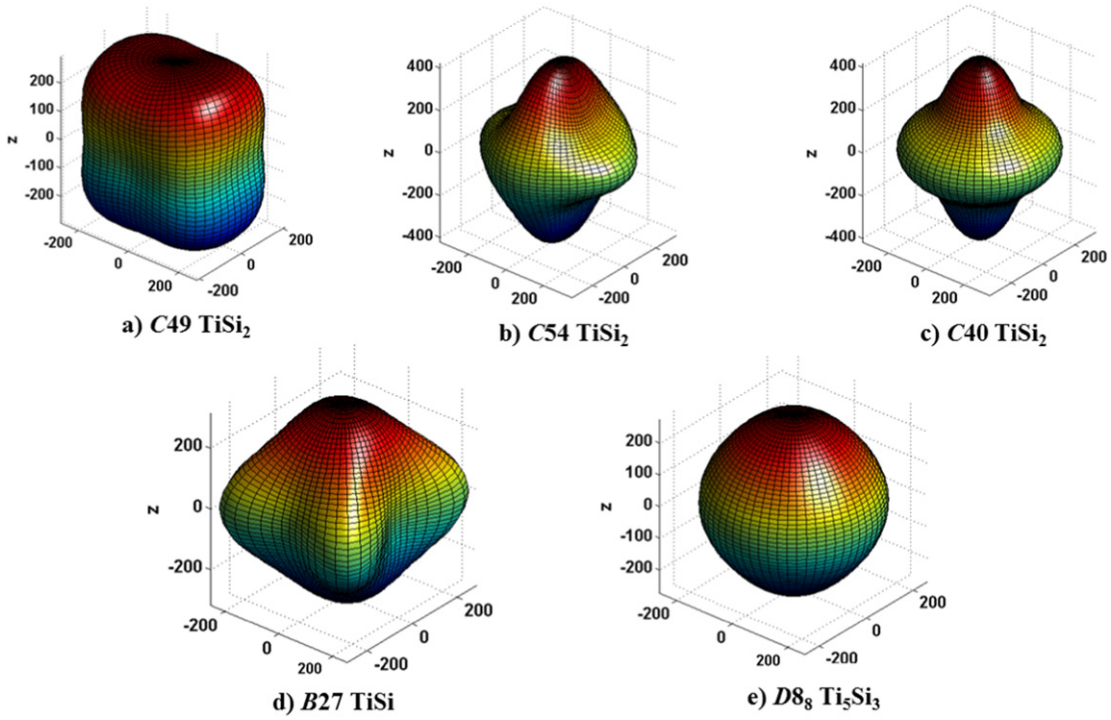

Figure 5. Direction dependent Young's modulus (E) of (**a**) $C49$ $TiSi_2$ (**b**) $C54$ $TiSi_2$ (**c**) $C40$ $TiSi_2$ (**d**) *Pnma* TiSi (**e**) Ti_5Si_3.

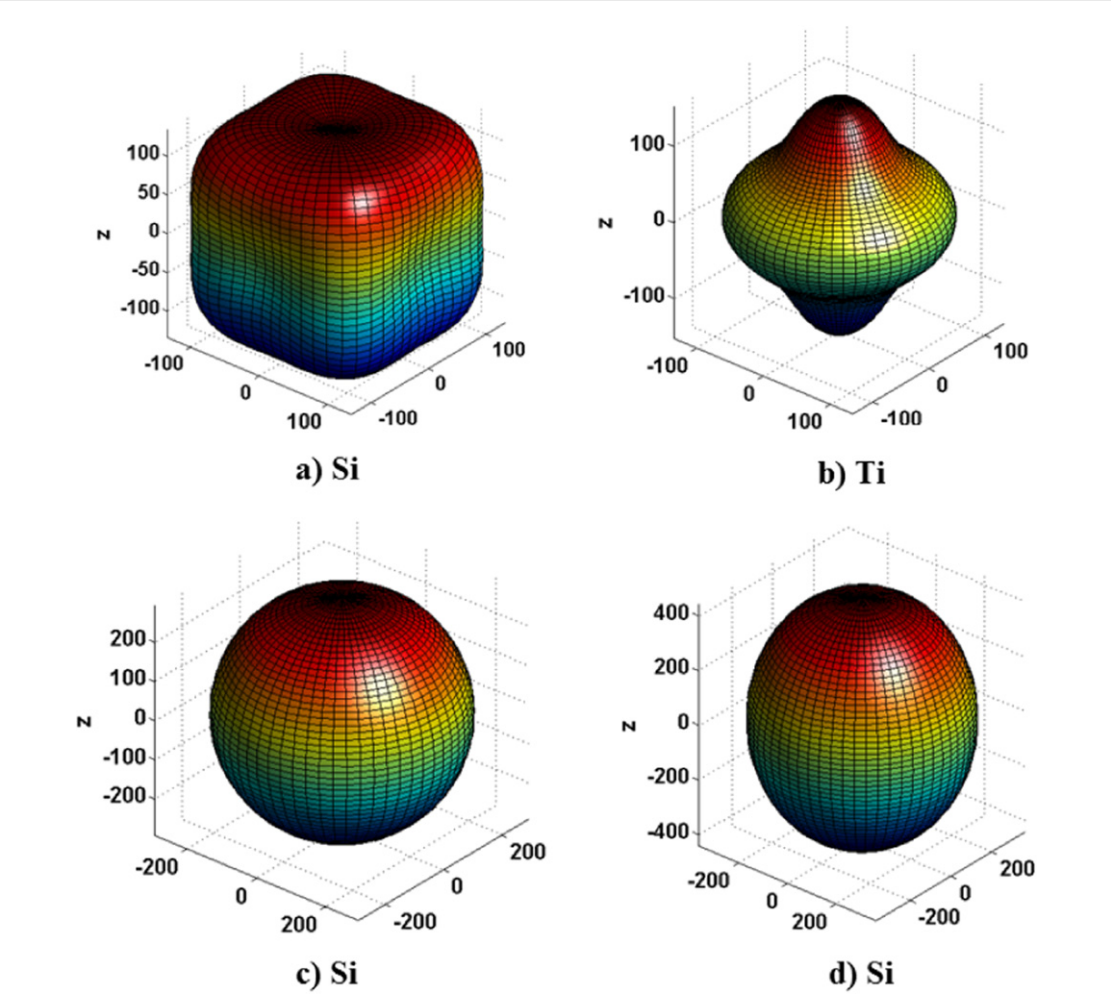

Figure 6. Directional Young's modulus (E) of (**a**) Si (**b**) Ti , directional bulk modulus (B) of (**c**) Si (**d**) Ti.

Table 7. Density (in 10^3 kg m^{-3}), longitudinal, transverse, and average sound velocities (in m s^{-1}), and Debye temperature of *C*49, *C*54, *C*40 $TiSi_2$, *Pnma* TiSi and Ti_5Si_3, Ti and Si.

		ρ	v_l	v_t	v_m	Θ_D (K)
C49 $TiSi_2$	GGA	4025	8269	5174	5699	699
C54 $TiSi_2$	GGA	4073	8622	5401	5948	732
C40 $TiSi_2$	GGA	4067	8610	5362	5909	727
Pnma TiSi	GGA	4239	8212	4925	5448	659
$D8_8$ Ti_5Si_3	GGA	4350	7896	4710	5214	623
Ti	GGA	4602	6243	3240	3626	417
	Exp.[32]	—	—	—	—	420
Si	GGA	2284	8723	5262	5818	634
	Exp.[32]	—	—	—	—	645

$$v_m = \left[\frac{1}{3}\left(\frac{2}{v_t^3} + \frac{1}{v_l^3}\right)\right]^{-1/3} \tag{20a}$$

where v_t and v_l are the transverse and longitudinal velocities in the polycrystalline material. v_t and v_l can be expressed in terms of polycrystalline bulk (B) and shear (G) moduli [43].

$$v_t = \left(\frac{G}{\rho}\right)^{1/2} \quad \text{and} \quad v_l = \left(\frac{3B + 4G}{3\rho}\right)^{1/2} \tag{20b}$$

The computed sound velocities and Debye temperatures of five Ti–Si systems are listed in table 7. The computed Debye temperature is 611 K for C49 $TiSi_2$, 508 K for C54 $TiSi_2$, 699 K for C40 $TiSi_2$, 659 K for *Pnma* TiSi, 623 K for Ti_5Si_3. The computed Debye temperatures for Ti and Si are 417 K and 635 K, and are in good agreement with experimental values of 420 K and 645 K [32].

8. Conclusion

The electronic structure and anisotropy in elastic properties are studied for five Ti–Si phases: *C*49 $TiSi_2$, *C*54 $TiSi_2$, *C*40 $TiSi_2$, *Pnma* TiSi and Ti_5Si_3. The density functional theoretical framework is used to compute elastic constants, elastic moduli, anisotropic factors, Debye temperature and sound velocities. The computed lattice parameters and fractional atomic coordinates are found to be in good agreement with available experimental values. The bonding in the Ti–Si phases is found to be mixed covalent–metallic type. The Young's modulus, shear modulus, Poisson's ratio and other elastic moduli of polycrystalline aggregates are computed from single crystal elastic constants. The anisotropy in elastic properties is estimated using shear anisotropic factors, bulk modulus anisotropic factors and directional Young's and bulk modulus. The elastic anisotropy in the Ti–Si phases may have significant implications for the mechanical properties, microstructure and growth of textured Ti–Si thin films on Si substrates.

Acknowledgements

This work was supported by the Department of Science and Technology (Grant No.: Sr/FTP/PS-179/2011), and the Center for Development of Advanced Computing (CDAC), Government of India.

References

[1] Chen L J (ed) 2004 *Silicide Technology for Integrated Circuits* (London: IEE)
[2] Tung R T 2014 *Appl. Phys. Rev.* **1** 011304
[3] Murarka S P 1983 *Silicides for VLSI Applications* (New York: Academic)
[4] Zhang S and Ostling M 2003 *Crit. Rev. Solid State Mater. Sci.* **28** 1
[5] Tung R T 2001 *Mat. Sci. and Eng.* R **1** 1–138
[6] Sze S M 1969 *Physics of Semiconductor Devices* (New York: Wiley)
[7] Niranjan M K and Waghnare U 2012 *J. Appl. Phys.* **112** 093702
[8] Senthilarasu S, Sathyamoorthy R and Lalitha S 2004 *Sol. Energy Mater. Sol. Cells* **82** 299–305
[9] Derrien J, Chevrier J, Lethanh V and Mahan J E 1992 *Appl. Surf. Sci.* **56–58** 382–93
[10] Rowe D M 1994 *CRC Handbook of Thermoelectrics* (Boca Raton: CRC Press) ch 23–25
[11] Jeon H, Sukow C A, Honeycutt J W, Rozgonyi G A and Nemanich R J 1992 *J. Appl. Phys.* **71** 4270
[12] Yu T, Tan S C, Shen Z X, Chen L W, Lin J Y and See A K 2002 *Appl. Phys. Lett.* **80** 2266

[13] La Via F, Mammoliti F, Corallo G, Grimaldi M G, Migas D B and Miglio L 2001 *Appl. Phys. Lett.* **78** 1864
[14] Li K, Chen S Y and Shen Z X 2001 *Appl. Phys. Lett.* **78** 3989
[15] Kittl J A, Prinslow D A, Apte P P and Pas M F 1995 *Appl. Phys. Lett.* **67** 2308
[16] Privitera S, La Via F, Grimaldi M G and Rimini E 1998 *Appl. Phys. Lett.* **73** 3863
[17] Chen S Y, Shen Z X, Li K, See A K and Chan L H 2000 *Appl. Phys. Lett.* **77** 4395
[18] Ekman M and Ozolins V 1998 *Phys. Rev.* B **57** 4419
[19] Ravindran P, Fast L, Korzhavyi P A, Johansson B, Wills J and Eriksson O 1998 *J. App. Phys.* **84** 4891
[20] Mattheiss L F and Hensel J C 1989 *Phys. Rev.* B **39** 7754
[21] Wang T, Oh S-Y, Lee W-J, Kim Y-J and Lee H-D 2006 *Appl. Surf. Sci.* **252** 4943–50
[22] Colinet C, Wolf W, Podloucky R and Pasturel A 2005 *Appl. Phys. Lett.* **87** 041910
[23] Nye F J 1985 *Physical Properties of Crystals* (Oxford: Oxford University Press)
[24] Wang T, Lee H-D, Oh S-Y, Kim Y-J and Lee W-J 2005 *Mater. Sci. Semicond. Process* **8** 540–4
[25] Kohn W and Sham L J 1965 *Phys. Rev.* **140** A1133
[26] Blochl P E 1994 *Phys. Rev.* B **50** 17953
[27] Giannozzi P *et al* 2009 *J. Phys.: Condens. Matter* **21** 395502 URL: (http://quantum-espresso.org)
[28] Perdew J P, Burke K and Ernzerhoff M 1996 *Phys. Rev. Lett.* **77** 3865
[29] CRC handbook of chemistry and physics 199576th edn ed D R Lide (Boca Raton: CRC Press)
[30] Michaelidis A and Scheffler M 2012 *Surface and Interface Science* vol 1 (New York: Wiley)
[31] Xu J-H, Oguchi T and Freeman A J 1987 *Phys. Rev.* B **35** 6940
[32] Kittel C 2004 *Introduction to Solid State Physics* 8th Edn (New York: Wiley)
[33] Birch E 1978 *J. Geophys. Res.* **83** 1257
[34] Niranjan M K 2012 *Intermetallics* **26** 150–6
[35] Hill R 1952 *Proc. Phys. Soc. London* **65** 350
[36] Voigt W 1928 *Lehrbuch der Kristallphysik* (Leipzig: Taubner)
[37] Reuss A 1929 *Z. Angew. Math. Mech.* **9** 55
[38] Pugh S F 1954 *Philos. Mag.* **45** 823
[39] Koster W and Franz H 1961 *Metall. Rev.* **6** 1
[40] Tvergaard V and Hutchinson J W 1988 *J. Am. Chem. Soc.* **71** 157
[41] Chung D H and Buessem W R 1968 *Anisotropy in Single Crystal Refractory Compound* ed F W Vahldiek and S A Mersol vol 2 (New York: Plenum) p 217
[42] Anderson O L 1963 *J. Phys. Chem. Solids* **24** 909
[43] Schreiber E, Anderson O L and Soga N 1973 *Elastic Constants and Their Measurements* (New York: McGraw-Hill)
[44] Jongste J F, Loopstra O B, Janssen G C A M and Radelaar S 1993 *J. Appl. Phys.* **73** 2816
[45] Lii K, Chen S Y and Shen Z X 2001 *Appl. Phys. Lett.* **78** 3989
[46] Pearson W, Villars P and Calvert L D 1985 *Pearson's Handbook of Crystallographic Data for Intermetallic Phases ~American Society for Metals* (OH: Metals Park)
[47] Farid B and Godby R W 1991 *Phys. Rev.* B **43** 14248
[48] Lu Z-W, Singh D and Krakauer H 1987 *Phys. Rev.* B **36** 7335
[49] Nakamura M 1993 *Metall. Trans.* A **25A** 331